Seismic fragility analysis of shear-critical concrete columns considering corrosion induced deterioration effects

Citation for published version:
Xu, JG, Wu, G, Feng, DC, Cotsovos, DM & Lu, Y 2020, 'Seismic fragility analysis of shear-critical concrete columns considering corrosion induced deterioration effects', *Soil Dynamics and Earthquake Engineering*, vol. 134, 106165. https://doi.org/10.1016/j.soildyn.2020.106165

Digital Object Identifier (DOI):
10.1016/j.soildyn.2020.106165

Link:
Link to publication record in Edinburgh Research Explorer

Document Version:
Peer reviewed version

Published In:
Soil Dynamics and Earthquake Engineering

Seismic fragility analysis of shear-critical concrete columns considering corrosion induced deterioration effects

Ji-Gang Xu[a], Gang Wu[a*], De-Cheng Feng[a], Demitrios M. Cotsovos[b], Yong Lu[c]

[a]Key Laboratory of Concrete and Prestressed Concrete Structures of the Ministry of Education, Southeast University, Nanjing 210096, China

[b]Institute of Infrastructure and Environment, School of Energy, Geoscience, Infrastructure & Society, Heriot-Watt University, Edinburgh EH14 4AS, United Kingdom

[c]Institute for Infrastructure and Environment, School of Engineering, The University of Edinburgh, Edinburgh EH9 3JL, United Kingdom

Abstract:

Shear-critical reinforced concrete structures such as older columns with insufficient transverse reinforcement details or short columns are found to be vulnerable to earthquake loading. Meanwhile, in the aggressive environment, RC structures tend to be more vulnerable to earthquake since corrosion of reinforcements will cause deterioration of the material properties. In the present study, a new framework is proposed for seismic fragility analysis of shear-critical structures with the consideration of corrosion effects. A new model for corroded concrete columns is proposed which can account for shear performance deterioration due to corrosion and the seismic flexure-shear interaction (FSI) behaviors. The modified Ibarra-Medina-Krawinkler deterioration model is adopted to simulate the shear response in order to capture shear strength and stiffness deterioration as well as pinching behavior of corroded shear-critical columns. The deteriorating material properties are determined based on corrosion modeling methods, and the corrosion level differences between transverse and longitudinal reinforcement are addressed. Furthermore, the proposed framework adopts time-variant structural capacities as obtained from the proposed numerical model in the fragility analysis. The developed framework is demonstrated with a shear-critical bridge column. The results clearly indicate the adverse effects of corrosion on seismic fragility of shear-critical columns, especially at severer damage states. Using flexure model and time-invariant capacity index will underestimate seismic fragility compared with the results obtained using the proposed method.

Keywords: Seismic fragility; reinforced concrete column; shear failure; flexure-shear interaction; corrosion effect

1. Introduction

Recent earthquakes have shown that the older reinforced concrete (RC) structures, such as buildings and bridges are vulnerable to earthquake actions [1-3]. These structures were either designed only considering gravity loads or not in accordance with the current generation of seismic codes as a consequence they are usually characterised by inadequate reinforcement details, such as insufficient transverse reinforcement for the columns. The insufficient detailing is particularly critical because it can potentially lead to premature shear failure of columns under seismic loadings. For example, many bridge columns designed with insufficient transverse reinforcement were found to fail in a shear manner which resulted in total collapse of the bridge structure during the 1971 San Fernando earthquake [2].

Shear failure has also been observed in short RC columns during earthquakes [2]. The post field investigations after the 2008 Wenchuan earthquake and the 2010 Yushu earthquake in China identified heavy damage being sustained by short columns in RC frames [4]. The poor seismic performance of concrete columns designed in accordance with the older generation of codes or short columns could be partially attributed to the complex flexure-shear interaction (FSI) behaviors under seismic cyclic loading conditions. The insufficient shear capacity and high shear demand of these columns usually lead to shear failure with limited ductility development. The failure of these shear-critical structures under earthquakes is generally more unexpected and catastrophic compared with flexure-dominated structures. As there are still many existing buildings or bridges located in high seismic areas [5, 6], which were not designed in accordance to current code specification, the development of a more reliable seismic performance evaluation method of these structures is imperative.

Aging and deterioration can also threat RC structural performance [7, 8]. Chloride-induced corrosion of reinforcement has been recognized as one of the main deterioration mechanisms affecting RC structural performance. For structures located in aggressive environment, the chloride ions penetration can induce corrosion of steel reinforcement, causing reduced effective sectional area and mechanical properties of steel bars, as well as the deterioration of the bond performance between reinforcing bars and concrete, the rust of steel corrosion can also induce concrete cracking and spalling of cover concrete. Therefore, the overall structural performance can be significantly affected by corrosion.

The joint effects of corrosion and seismic hazard on RC structures have been subject of much research interest in more recent years. Many studies have been conducted to develop suitable methods towards life-cycle seismic fragility analysis or reliability assessment of RC structures considering corrosion induced deterioration effects [9-15]. The research conducted by Choe et al. [9, 10] highlighted the adverse effects of corrosion on seismic fragility and reliability of a typical single-bent bridge. The work of Ghosh and Padgett [16] dealt with the aging effects on bridge system seismic fragility. For frame structures, relevant studies [7, 15, 17-19] have also indicated that corrosion could detrimentally affect the structural seismic performance.

However, most of the existing studies regarding the combined effects of corrosion and seismic hazard on RC structural performance only focused on structures of which the behaviour was dominated by flexure failure mode, while limited attention has been paid on corroded structures with shear-critical components which could be particularly vulnerable to earthquake loading [20, 21]. On the other hand, a reliable seismic analysis of corroded shear-critical structures requires an efficient analytical model capable of realistically capturing shear performance deterioration due to corrosion and the complex flexure-shear interaction behaviors observed under seismic actions. Although there are many studies aiming to develop modeling methods for uncorroded concrete columns that could consider FSI behaviors [22-26], very few studies accounted for shear capacity deterioration and seismic FSI behaviors of corroded concrete columns [27]. A very recent study conducted by Zhang et al. [21] has developed a modeling approach for corroded shear-critical columns. The approach is based on the method proposed by Elwood [28] for uncorroded columns and the use of modified material properties to incorporate corrosion deterioration effects; however, the model cannot account for the complex hysteric behaviors such as basic cyclic strength deterioration as well as pinching since the hysteric model in their approach is fixed [29].

In view of the life-cycle context of seismic performance assessment of RC structures, appropriate consideration of the corrosion process on structural performance is important. In reality, the transverse and longitudinal reinforcements will suffer different corrosion levels over time [30, 31], due to their different distance to the cover concrete surface (exposure surface) and the smaller diameter of transverse reinforcements with respect to longitudinal reinforcements. This can result in variant deterioration rates of shear capacity and flexure performance which have not been appropriately considered in existing studies. In fact, some studies assign the same corrosion levels on transverse and longitudinal reinforcement [21], and this may result in bias results of seismic performance assessment when shear performance and/or FSI behavior is considered. On the other hand, research investigating the seismic fragility assessment of corroded structures has found that the structural capacity is time-variant and should be considered since using original capacity index will generally underestimate structural seismic fragility [15, 16, 32]. Although some studies have investigated the variance of the structural capacity index and incorporated them into time-dependent seismic fragility analysis of structures with flexure-dominated behaviour [16, 32], few studies have incorporated the time-dependent structural capacity into seismic fragility analysis of shear-critical structures considering corrosion induced deterioration effects.

Addressing the above drawbacks, a new framework is proposed herein to conduct time-dependent seismic fragility analysis for shear-critical RC structures considering corrosion induced deterioration effects. A new numerical modeling methodology for corroded RC columns is developed which could account for shear capacity deterioration and FSI behaviors. The model is developed in OpenSees [33] using a macro-element modeling concept. The flexural response is modelled by a fiber-based beam-column element, while the slip response is modelled by a zero-length fiber section element. A new zero-length spring element is introduced to account for the shear response. The hysteretic behavior of the shear element is modelled by the modified Ibarra-Medina-Krawinkler deterioration model [34, 35] in order to capture shear strength and stiffness deterioration as well as pinching behavior of corroded columns. The proposed model is validated by comparing the simulation results with the experimental data for several shear-critical columns. The framework also comprises a corrosion modeling part which aims to compute the time-dependent material properties and especially accounts for the corrosion level differences of transverse and longitudinal reinforcements over time. The time-variant structural capacity is defined based on the proposed numerical model and then incorporated into the seismic fragility analysis. A shear-critical bridge column is selected to demonstrate the proposed fragility analysis framework. The effects of corrosion on seismic fragility curves are discussed. Finally, the influences of the modeling method and the time-variant capacity on analysis results are also discussed.

2. Corrosion induced deterioration modeling

For RC structures located in an aggressive environment, chloride ions can ingress the concrete cover, depassivate the steel reinforcement and initiate corrosion after a certain time. Subsequently, the mechanical properties of the steel reinforcement bars and the concrete will degrade over time and as a result, structural performance will deteriorate. In this section, the method adopted for modeling corrosion initiation and propagation will be discussed, and the determination of the deteriorating material properties with time is also presented.

2.1 Initiation Phase

Generally, corrosion initiates when the chloride concentration around the steel reinforcement exceeds a critical threshold value. In the present study, the probabilistic model proposed by Choe et al. [10] is adopted for simulating the corrosion initiation time T_0 (year), which is expressed as:

$$T_0 = X_I \left\{ \frac{x_c^2}{4k_e k_t k_c D_0 t_0^n} \left[\mathrm{erf}^{-1} \left(\frac{C_s - C_{cr}}{C_s} \right) \right]^{-2} \right\}^{\frac{1}{1-n}} \tag{1}$$

where X_I is the model uncertainty factor, and taken as 1.0; x_c is the concrete depth and will be taken differently for transverse and longitudinal reinforcement based on the actual reinforcement configuration of the column; k_e, k_t and k_c are environment factor, test factor and curing factor, respectively; D_0 is the diffusion coefficient; t_0 is the reference time; n is the aging factor; C_s and C_{cr} are the equilibrium chloride concentration and the critical chloride concentration at the concrete surface, respectively; $\mathrm{erf}^{-1}(\cdot)$ is the Gaussian error function. Detailed values of the above parameters will be given in the case study section later.

2.2 Propagation Phase

Following the corrosion initiation, the propagation phase should be simulated in order to determine the actual level of corrosion characterising the steel reinforcement bars. The corrosion rate model proposed by [9] is adopted for uniform corrosion cases under consideration:

$$r_{cr}(t) = \frac{32.13(1-w/c)^{-1.64}}{x_c}(t-T_0)^{-0.29} \tag{2}$$

where $r_{cr}(t)$ is the corrosion rate at time t; w/c is the water to cement ratio.

Based on this time-dependent corrosion rate model, the erosion depth $e_{cor}(t)$ can be calculated through integrating the corrosion rate:

$$e_{cor}(t) = 0.0116\int_{T_0}^{t} r_{cr}(t)dt = \frac{0.5254(1-w/c)^{-1.64}}{x_c}(t-T_0)^{0.71} \tag{3}$$

Because of the corrosion, the cross-sectional area of steel reinforcement reduce over time. After corrosion initiation ($t \geq T_0$), the time-dependent diameter d_{cor} of steel reinforcement can be calculated as:

$$d_{cor}(t) = d_0 - 2e_{cor}(t) \tag{4}$$

where d_0 is the diameter of the original uncorroded steel reinforcement. Therefore, the corrosion level of steel reinforcement at time t can be calculated as:

$$X_{cor}(t)=\frac{d_0^2-d_{cor}^2(t)}{d_0^2}\times 100\% \tag{5}$$

where X_{cor} is the corrosion level determined in terms of percentage of mass loss.

2.3 Material properties deterioration due to corrosion

2.3.1 Steel reinforcements

Based on available experimental results [36, 37], the mechanical properties of corroded steel reinforcements will degrade in terms of yielding strength, elastic modulus, ultimate strength and strain, as shown in Fig. 1. The present study adopts the empirical formulae proposed by [38] for corroded steel reinforcement properties evaluation:

$$f_{y,cor}(t)=f_{y0}(1-\alpha_1 X_{cor}(t)) \tag{6}$$

$$f_{u,cor}(t)=f_{u0}(1-\alpha_1 X_{cor}(t)) \tag{7}$$

where $f_{y,cor}$ and $f_{u,cor}$ are the yielding and ultimate strength of corroded steel reinforcements, respectively; f_{y0} and f_{u0} are the yielding and ultimate strength of the uncorroded steel reinforcements, respectively; α_1 is the empirical parameter and taken as 0.005 based on [37].

Similarly, the elastic modulus and ultimate strain can be calculated as [38]:

$$E_{s,cor}(t)=E_{s0}(1-\alpha_2 X_{cor}(t)) \tag{8}$$

$$\varepsilon_{u,cor}(t)=\varepsilon_{u0}(1-\alpha_3 X_{cor}(t)) \tag{9}$$

where $E_{s,cor}$ and $\varepsilon_{u,cor}$ are the elastic modulus and ultimate strain of corroded steel reinforcements, respectively; E_{s0} and ε_{u0} are the elastic modulus and ultimate strain of uncorroded steel reinforcements, respectively; α_2 and α_3 are the empirical parameters and taken as 0.01 and 0.05 [36], respectively.

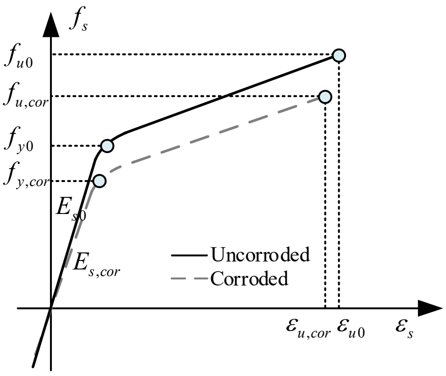

Fig. 1. Mechanical properties of steel reinforcements.

2.3.2 Concrete properties

Effects of corrosion on concrete properties are evaluated for cover unconfined concrete and confined core concrete separately, as shown in Fig. 2. For the cover unconfined concrete, steel rust due to corrosion will cause volumetric expansion and develop splitting stresses in concrete, as a result the concrete strength will degrade. The reduced cover concrete strength can be calculated as:

$$f_{c,cor}=\zeta f_{c0} \tag{10}$$

where $f_{c,cor}$ and f_{c0} are the compressive strength of corroded and uncorroded concrete, respectively; ζ is the softening coefficient which can be calculated by [39]:

$$\zeta = \frac{0.9}{\sqrt{1+600\varepsilon_{cr}}} \tag{11}$$

$$\varepsilon_{cr} = \sum w_{cr} / b_0 \tag{12}$$

where ε_{cr} is the average tensile strain in cracked concrete; b_0 is the initial width of the concrete cross-section; w_{cr} is the crack width induced by corrosion of each reinforcement, which is calculated as:

$$w_{cr} = 2\pi(v_{cr} - 1)e_{cor}(t) \tag{13}$$

where v_{cr} is the ratio of the volumetric expansion due to steel corrosion, and is taken as 2.0 in this study [40].

For the core confined concrete, the confinement effect of transverse reinforcement will deteriorate because of corrosion. In this study, the modified Kent-Park confined concrete model [41] is adopted for simulating the confined concrete properties:

$$K = 1 + \frac{\rho_{st,v} f_{yt,cor}}{f_{c0}} \tag{14}$$

$$f^{'}_{cc,cor} = K f_{c0} \tag{15}$$

$$\varepsilon_{cc,cor} = K\varepsilon_{c0} \tag{16}$$

where K is the confinement ratio; $\rho_{st,v}$ is the volume ratio of the corroded transverse reinforcement; $f_{yt,cor}$ is the yielding strength of the corroded transverse reinforcement; $f^{'}_{cc,cor}$ is the compressive strength of the core confined concrete; $\varepsilon_{cc,cor}$ is the peak strain corresponding to the concrete strength.

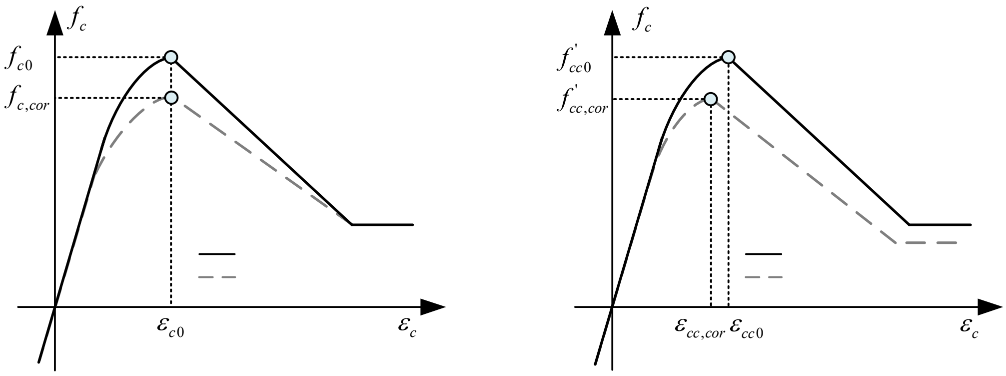

Fig. 2. Mechanical properties of concrete: (a) cover concrete; (b) core concrete.

3. Proposed modeling methodology for corroded shear-critical columns

A two-dimensional (2D) nonlinear FE model is developed in OpenSees [33] for simulating seismic behavior of corroded reinforced concrete columns. As illustrated in Fig. 3, a fiber based beam-column element is used for flexure response simulation; a zero-length spring element is used for shear response simulation and a zero-length fiber section element is used for rotational slip response simulation. In this way, the flexure response, shear response are all well considered and coupled at the element level.

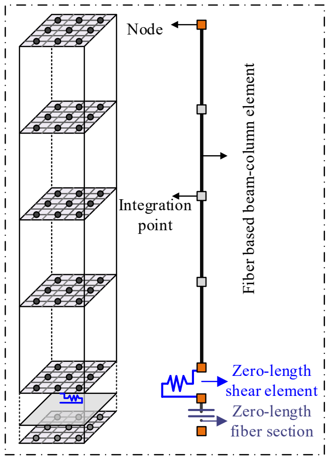

Fig. 3. Proposed modeling concept for corroded columns considering flexure-shear interaction (FSI).

3.1 Flexure response

The flexure response of the corroded column is modelled with a beam-column element assigned with a fiber section. The fiber section is divided into concrete fibers and steel fibers with unique constitutive stress-strain relationship. However, as discussed before, because of the corrosion of steel reinforcement, the mechanical properties of steel and concrete will deteriorate. Thus, the time-dependent deteriorated constitutive stress-strain relationship of steel and concrete fibers are used for corroded concrete column. Besides, the material *Steel02* and *Concrete01* in OpenSees are adopted for simulating the steel reinforcements and concrete fibers, respectively.

3.2 Rotational slip response

Because of the strain penetration or bond slip of the longitudinal reinforcing bars anchored into the column footing, additional column end rotation, and hence lateral displacement, could be generated due to rigid body rotation. This phenomenon could be more significant for corroded columns as corrosion will also reduce bond strength of longitudinal bars [42, 43]. In order to capture this behaviour, a zero-length fiber section element is added at the column-footing interface for slip response simulation. This element adopts the same fiber configuration with the flexure beam-column element but with different stress-strain relationship for steel fibers. The *Bond_SP01* strain penetration model proposed by Zhao and Sritharan [44] is adopted and modified for steel fibers:

$$S_y\,(\mathrm{mm}) = 2.54\left[\frac{d_{l,cor}\,(\mathrm{mm})}{8437}\frac{f_{yl,cor}\,(\mathrm{MPa})}{\sqrt{f_{c0}}\,(\mathrm{MPa})}(2\alpha+1)\right]^{1/\alpha} + 0.34 \tag{17}$$

where $d_{l,cor}$ and $f_{yl,cor}$ are the diameter and yielding strength of corroded longitudinal rebar, respectively; f_{c0} is the concrete strength; α is a parameter and taken as 0.4. In case of ultimate slip S_u, it is taken as $35S_y$ for all corrosion situations for simplicity [45]. Especially, in order to maintain compatibility between the beam-column element and the slip section element, the ultimate strain of concrete fibers is multiplied by a scale factor F_k, more details can be found in [46].

3.3 Shear response

A zero-length shear spring element is added at the end of the column for shear response simulation. Corroded shear-critical columns may experience shear failure under seismic loading, leading to significant deterioration in terms of strength, unloading and reloading stiffness, as well as pinching. Thus, the shear spring element should have the ability to represent the complex degradation behaviors of the corroded columns.

In this investigation, the modified Ibarra-Medina-Krawinkler deterioration model (IMK) [34, 35] is used to simulate the shear response of the corroded columns. Fig. 4 shows the skeleton curve of the IMK deterioration model. The skeleton curve has three characteristic points: yielding shear strength V_y and deformation Δ_y; peak shear strength V_n and deformation Δ_n; residual shear strength V_r ($V_r = 0.2V_n$) and deformation Δ_r. Two additional deformation parameters, namely pre-peak plastic deformation Δ_p and post-peak deformation Δ_{pc}, can be calculated from the three basic characteristic points, as shown in Fig. 4.

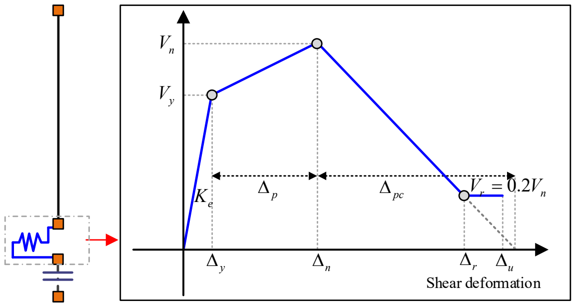

Fig. 4. Skeleton curve of the IMK hysteretic model.

In order to represent the pinching phenomenon of the columns, the IMK model with pinched response is selected in this study. Fig. 5 shows the basic hysteretic rule of the IMK model with pinched hysteretic response. The parameter $\kappa_{\mathrm{f,d}}$ defines the ratio of the load at which reloading begins to the load that corresponds to the maximum historic deformation demand, while the pinching related parameter a_p (*APinch* in OpenSees) defines the ratio of reloading stiffness. A smaller a_p value indicates more significant pinching behavior. More details of the model can be found in [34, 35].

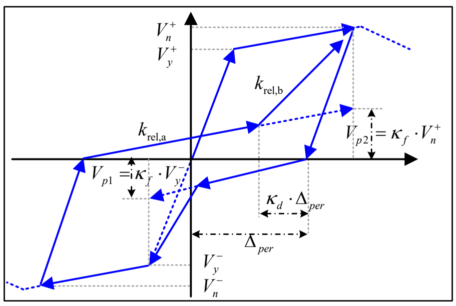

Fig. 5. Basic hysteretic model rules with pinched response (adapted from Ibarra et al. [34]).

4. Development of IMK-based shear hysteretic model

4.1 Pre-peak behaviour

The modified compression field theory (MCFT) developed by Vecchio and Collins [47] has been used by many studies [48-51] to simulate the shear response of reinforced concrete columns, and the results indicated good predictions compared with experimental test results. Thus in this study, the MCFT is adopted for determining the pre-peak modeling parameters on the curve of the IMK model. The MCFT has been implemented in the software Response-2000 [52] which can be easily used for shear response calculation. However, it is difficult to represent the deteriorated cover concrete by using different concrete materials for cover concrete and confined concrete, thus, instead of using different concrete strength, the thickness of cover concrete of corroded columns is modified as:

$$\frac{t_c^{'}}{t_c} = \frac{f_{c,cor}}{f_{c0}} = \zeta \tag{18}$$

where t_c and $t_c^{'}$ are cover concrete depth for uncorroded and corroded columns, respectively. Fig. 6 illustrates the reduced section of corroded column.

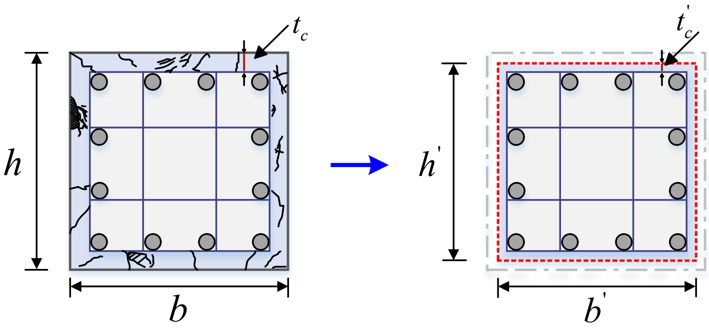

Fig. 6. Section dimension reduction for corroded columns.

The shear response of column section will change due to the varation of the bending moment along the column length. In order to consider this flexure-shear interaction effect on column shear response, the method proposed by Xu and Zhang [50] is aopted in this study. The column is divided into several elements and the shear response is calculated individually for each element based on the average moment to shear ratio corresponding to each element. The overall shear force-shear displacement is obtained by interagting the shear response along the column length. More detalis can be referred to [50].

The calculated pre-peak shear force-shear displacement response from MCFT is then simplified into two linear segments, so as to correspond to the IMK model. The two characteristic points of the simplified relationship are yield shear strength and peak shear strength as shown in Fig. 7. Referring to Sezen and Moehle [53], the yield shear strength is defined as the intersection point of the line corresponding to the secant stiffness at 70% of the peak shear force and the horizontal line passing peak shear strength at the skeleton curve.

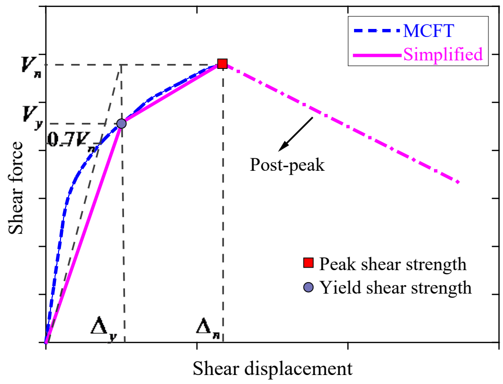

Fig. 7. Determination of skeleton curves of shear response.

4.2 Post-peak negative stiffness

Although the MCFT can calculate the pre-peak shear response of columns with good accuracy, it cannot obtain stable post-peak response due to its force-based approach [50]. Thus some studies assumed zero tangential stiffness response for post-peak stage [49, 50]. Although with this simplification the reloading stiffness deterioration can be simulated, the post-peak strength deterioration behavior cannot be represented. In this paper, the post-peak stiffness is defined by the model proposed by Baradaran Shoraka [54], in order to generate a composed skeleton curve including post-peak deterioration stage as shown in Fig. 7.

The total post-peak stiffness $K_{\deg}^{t}$ of the column is defined by the shear-friction based mechanical model proposed by Baradaran Shoraka [54] as:

$$K_{\deg}^{t} = -4.5P(4.6\frac{A_{st,cor}f_{yt,cor}d_c}{Ps}+1)^2 / L \tag{19}$$

where P is the axial load; $A_{st,cor}$ is the area of transverse reinforcement; d_c is the depth of the column core; s is the transverse reinforcement spacing and L is the column length.

Then the post-peak stiffness $K_{\deg}$ of the shear spring can be calculated with the method proposed by Elwood [28]:

$$\frac{1}{K_{\deg}} = \frac{1}{K_{\deg}^{t}} - \frac{1}{K_{unload}} \tag{20}$$

where K_{unload} is the flexural unloading stiffness, which could be taken equal to the initial flexural stiffness.

4.3 Hysteretic deterioration modeling

The proposed procedure discussed above defines the skeleton curve of the shear response of corroded columns, which bounds the shear strength. However, cyclic loading could result in additional deterioration effects on shear response [55, 56], e.g., the in-plane cyclic strength deterioration phenomenon [57], which should be reasonably considered.

The IMK model uses the hysteretic energy based cyclic deterioration rules developed by Rahnama and Krawinkler [58] to define cyclic deterioration rates for strength and stiffness:

$$\beta_i = \left(\frac{E_i}{E_t - \sum_{j=1}^{i-1} E_j} \right)^c \tag{21}$$

where E_i is the dissipated energy of excursion *i*; *c* is an empirical parameter and can be taken as 1.0; E_t is the reference hysteretic energy dissipation capacity of the structural component:

$$E_t = \gamma F_y \Delta_y \tag{22}$$

Then the strength and/or stiffness deterioration rate can be calculated as:

$$F_i = (1 - \beta_i) F_{i-1} \tag{23}$$

where F_i, F_{i-1} are strength and/or stiffness before and after cyclic excursion *i*.

The parameter γ defines the hysteretic energy dissipation capacity of structural components and can be calibrated from experimental results. The value for this parameter can be set uniformly for different deterioration modes [34, 35]. In this paper, the empirical relationship proposed by Wang et al. [59] is adopted for defining γ :

$$\gamma = \begin{cases} 600 & a/d \le 2 \\ 400a/d - 200 & 2 < a/d \le 3 \\ 1000 & a/d > 3 \end{cases} \tag{24}$$

where *a/d* is the ratio of column shear span *a* to section depth *d*.

5. Validation of the proposed numerical modeling approach

In this section, the proposed modeling method will be validated through simulating three shear-critical columns under cyclic loading. Meanwhile, to further demonstrate the importance of incorporating FSI, the columns are also simulated with only flexure response considered. The selected columns include an uncorroded column and two corroded columns which all failed in shear. Table 1 lists the basic information of the selected columns. Fig. 8 shows the shear force-shear displacement response obtained from MCFT of the columns. Table 2 lists the IMK modeling parameters of each column, where γ is defined from Eq. 24, a_p is set as 0.2 for all columns, $\kappa_{f,d}$ is set as 0.5 for specimen S1 and COR_1, and 0.3 for C5 as this column shows significant pinching response.

Table 1
Basic information of selected columns.

Specimen	S1	C5	COR_1
Reference	Sezen and Moehle [60]	Vu and Li [31]	Lee et al. [61]
Column length (mm)	2946	1780	1100
Section $b \times h$ (mm×mm)	457×457	350×350	300×300
Shear span to depth ratio a/d	3.74	3.18	2.29
Axial load P (kN)	667	958	705
Concrete strength f_c (MPa)	21.1	31.3	39.2
Longitudinal bars (mm)	8Ø28.7	8Ø20	12Ø16
Yield strength f_{yl} (MPa)	438	550	362
Transverse bars (mm)	Ø28.7@305	Ø7.8@50	Ø10@80
Yield strength f_{yt} (MPa)	476	300	347
Corrosion level-transverse (%)	-	15.5	6.8
Corrosion level-longitudinal (%)	-	3.9	-

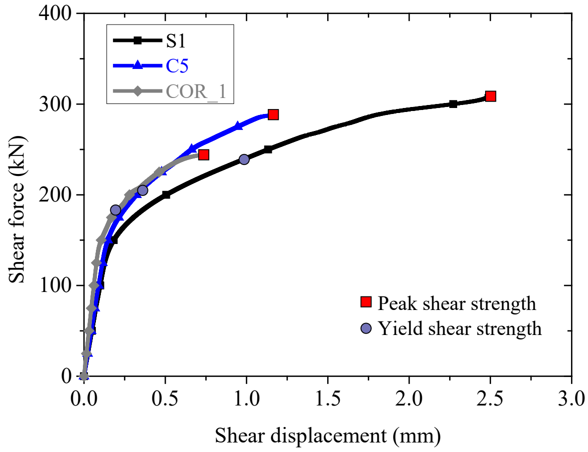

Fig. 8. Shear force-shear displacement for selected shear-critical columns.

Table 2
IMK modeling parameters of selected columns.

Specimen	γ	κ	a_p
S1	1000	0.5	0.2
C5	1000	0.3	0.2
COR_1	760	0.5	0.2

Fig. 9 shows the modeling results for specimen S1, where Fig. 9(a) is the comparison of skeleton curves of shear response, flexure response and total response including FSI with the experimental result, and Fig. 9(b) is the comparison of hysteric responses of flexural simulation alone, combined flexure and shear simulation (labelled as “FSI simulation”), and the experimental result. It should be noted that this column was designed with inefficient transverse reinforcement and hence failed in shear under cyclic loading during the test.

It can be seen that the flexural simulation slightly overestimates the initial stiffness and peak lateral strength. Meanwhile, the flexural simulation cannot well capture cyclic deterioration behavior. The flexure simulation significantly overestimates the strength and stiffness after peak strength. One possible reason could be that the flexure model in this study ignored the inleastic buckling and low-cycle fatigue of longitudinal bars [62, 63]. While the combined flexure and shear simulation, which in this case is dominated by the shear response, can provide good predictions as compared with the test result. The post-peak deterioration response can be well simulated by the proposed numerical method, the pinching phenomenon can also be effectively modelled by the proposed method.

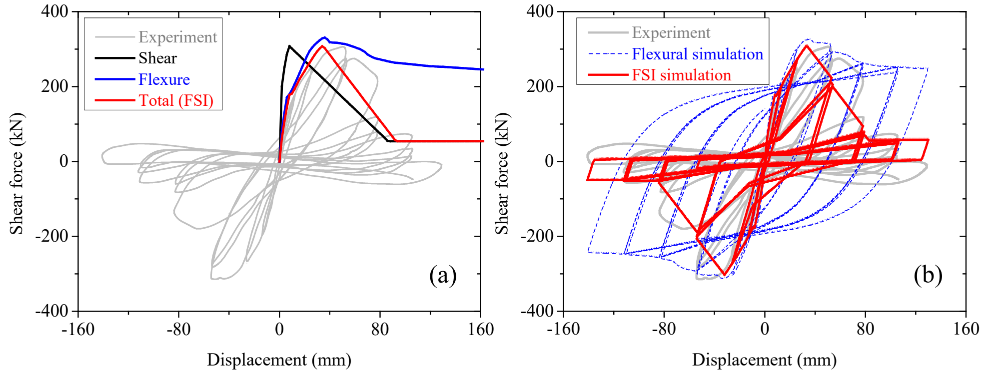

Fig. 9. Comparison of simulated and test results for specimen S1: (a) skeleton curves; (b) cyclic hysteric response.

Fig. 10 illustrates the modeling results for specimen C5. This column was originally ductile-designed, but finally failed in shear due to transeverse reinforcement corrosion. It can be seen that the peak shear strength is slighltly over predicted with MCFT. However, comparaed with flexural simulation, the overall hysteric response, inclduing post-peak strength and stiffness deterioration and the overall pinching behavior from flexure-shear simulation are more close to test result.

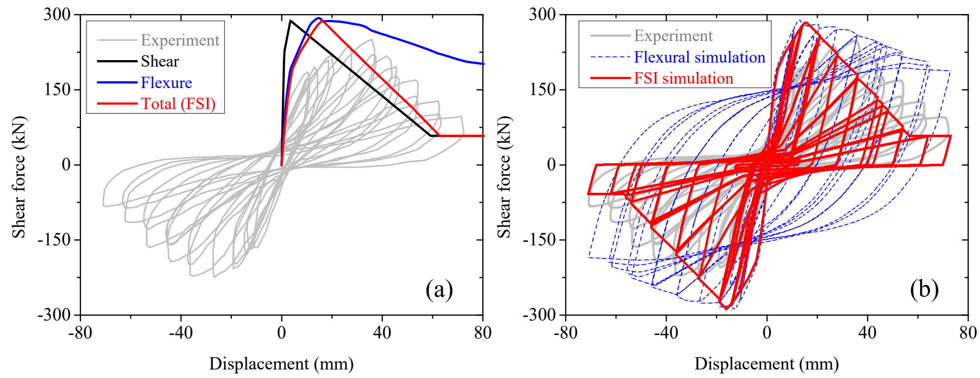

Fig. 10. Comparison of simulated and test results for specimen C5: (a) skeleton curves; (b) cyclic hysteric response.

The modeling results of specimen COR_1 are shown in Fig. 11. This column was a short shear-critical column as the shear span to section depth ratio was 2.3, and the column was only corroded in the transverse reinforcement, resulting in a shear failure during the test. It can be seen from Fig. 11 that, overall, the proposed model can appropriately simulate the reloading and unloading branches in terms of the strength and stiffness, as well as pinching behavior. The peak shear strength is well predicted and the significant post-peak deterioration response is also well captured. Once again, the flexural simulation significantly overestimates the post-peak response, including strength and reloading stiffness.

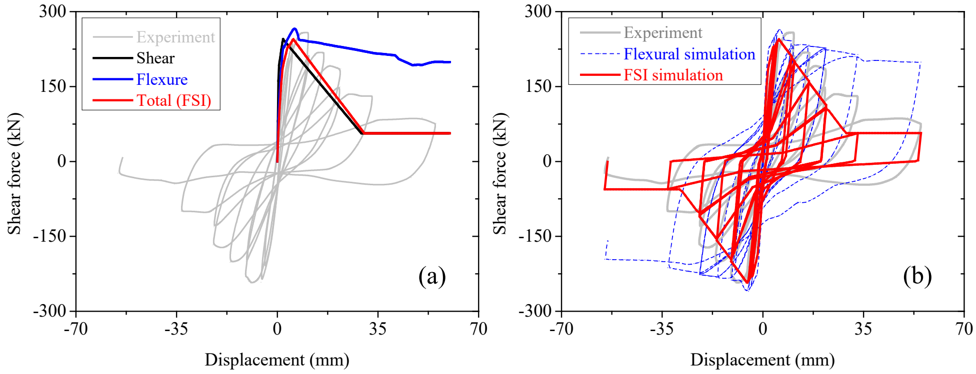

Fig. 11. Comparison of simulated and test results for specimen COR_1: (a) skeleton curves; (b) cyclic hysteric response.

6. Framework for time-dependent seismic fragility assessment

Adopting the numerical modeling methodology proposed herein for realistically describing FSI which characterised the behaviour of corroded RC columns, the time-dependent seismic fragility of shear-critical RC columns can be analyzed. Fig. 12 shows a flowchart providing a concise description of the process followed for conducting seismic fragility analysis of shear-critical RC structures when considering corrosion induced deterioration effects. The first major step is to check whether or not corrosion initiates at a given year under consideration; if corrosion initiates, the deteriorated material properties will be computed. The second major step is to develop a numerical analysis model realistically representing the structures considered using the proposed method described earlier. The final major step is to conduct the seismic vulnerability analysis of the structures considered. This step includes structural capacity analysis that defines the time-dependent structural limit states, and the development of seismic demand model of interested engineering demand parameter (EDP). In this study, the seismic demand model is obtained using the incremental dynamic analysis (IDA) [64] method. More details are provided in the case study presented in section 7.

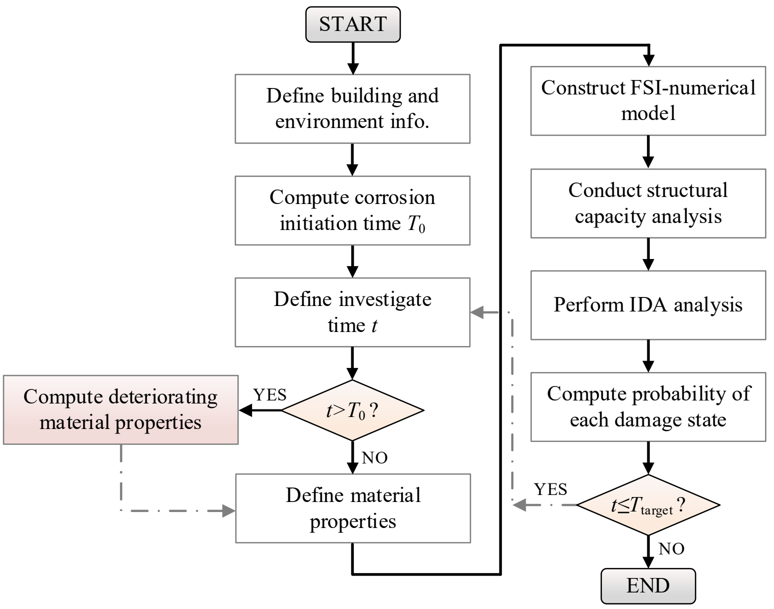

Fig. 12. Flowchart of time-dependent seismic fragility analysis of structures.

7. Case study

7.1 Prototype bridge column

A shear-critical bridge column is selected from a typical two span continuous box-girder bridge which has been in service for many years [51]. This bridge has not been designed in accordance to current code specification, and is representative of older bridges in southern California constructed prior to 1970s. The bridge column is 6553mm in length and the column section is shown in Fig. 13. The shear span to depth ratio is 3.6 for both of the longitudinal direction (double curvature bending) and transverse direction (single bending), and the transverse reinforcement spacing of the column is 305mm. With these design details, the column can be considered as a shear-critical column as checked by Jeon et al. [51]. The cover thickness is 30mm, and the diameter of longitudinal rebar is 36mm and that of transverse reinforcement is 13mm. The concrete strength is 27MPa and the yield strength of the steel reinforcement is 303MPa. The assumed exposure condition of the bridge is the marine tidal-zone, wherein the bridge column is subjected to alternate wetting and drying cycles from the sea water containing chloride, which is considered to be a major deterioration mechanism for bridge columns.

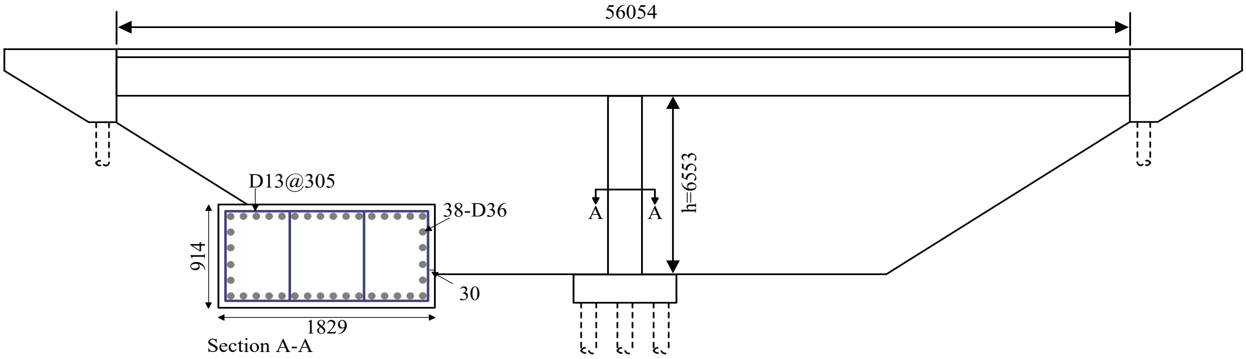

Fig. 13. Schematic diagram of the bridge column (all dimensions are in mm).

7.2 Corrosion modeling

For the assumed exposure condition of the bridge, the parameters introduced into the corrosion initiation model are adopted from [9] as shown in Table A-1 in Appendix A. For these parameters, the calculated corrosion initiation time for transverse reinforcement is 5.6 years, and it increases to 17.3 years for longitudinal reinforcement due to the thicker embedded depth. After corrosion initiates, the time-dependent deteriorating material properties can be computed with the method discussed in Section 2.3. Fig. 14(a) shows the corrosion levels for the longitudinal and transverse reinforcement, respectively. It can be clearly seen that the two types of reinforcement will suffer different corrosion levels over time. For instance, the corrosion levels of transverse reinforcement are 12.8%, 23.3% and 37.9% at 25 year, 50 year and 100 year, respectively; while the corresponding corrosion levels of longitudinal reinforcement will be 1.8%, 5.1% and 9.5%. The time-dependent yield strength of the reinforcements is shown in Fig. 14(b). The figure indicates that the transverse reinforcement has a higher deterioration rate of yielding strength than longitudinal reinforcement.

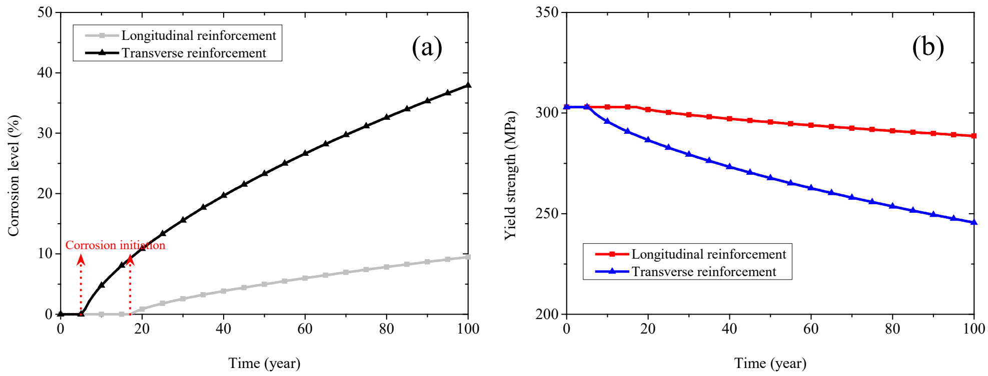

Fig. 14. Corrosion modeling results for transverse and longitudinal reinforcements: (a) corrosion levels; (b) yield strength.

7.3 Structural capacity assessment

The bridge column is then modelled using the proposed method which could consider the shear performance deterioration and the FSI behaviors. It should be noted that only the longitudinal direction response of the column are analysed in the present study. The effects of corrosion induced deterioration on structural capacity are assessed in this section. Fig. 15 shows the calculated shear force-shear strain relationship of the column at different investigated times. It can be seen that the peak shear strength reduces over time and the ultimate shear deformation capacity also decreases.

With the developed numerical models, the static push-over analysis is conducted on the column. Fig. 16(a) shows the obtained monotonic curves of the column at different investigated times. It can be seen that the initial stiffness will slightly decrease while the yielding strength and peak shear strength show significant reduction as the corrosion time increases. As a comparison, the static push-over analysis are also conducted using the flexure-models and the results are presented in Fig. 16(b). Comparing the two figures, it can be seen that the column will have lower peak lateral strength and more pronounced post-peak softening response if the FSI is considered.

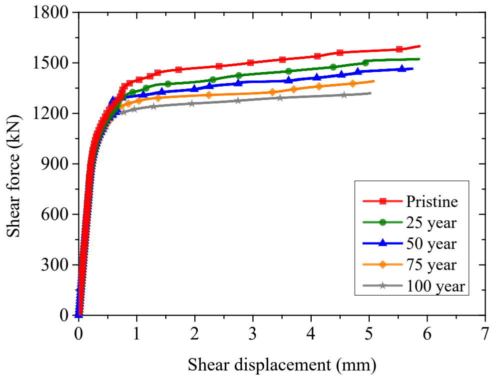

Fig. 15. Shear force-shear displacement relationship for the column.

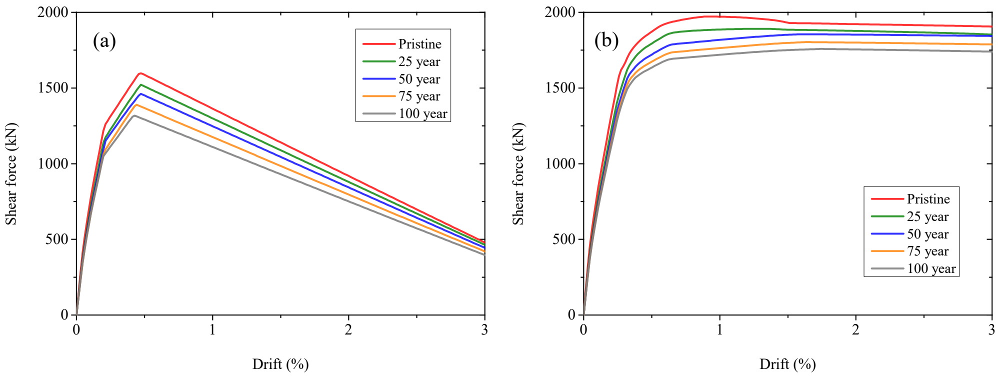

Fig. 16. Computed monotonic curves of the column using two modeling approaches: (a) based on FSI-model; (b) based on flexure model.

As mentioned before, although some previous studies have addressed the importance of incorporating time-variant structural capacity in seismic fragility analysis, few studies have tried to investigate the variation of structural capacity of shear-critical columns while also considering the effect of corrosion and incorporating them into a time-dependent seismic fragility analysis. Based on the proposed FSI-model for columns, the structural capacity of the columns can be obtained based on push-over curves. In this study, four limit states are defined as follows: slight damage (SD); moderate damage (MD); extensive damage (ED) and collapse prevention (CP). As shown in Fig. 17, MD is defined as having a drift ratio corresponding to yield shear strength of the column, while SD is defined as having half of the drift ratio of MD. ED is defined as having a drift ratio corresponding to the peak shear strength, and finally CP is defined as reaching a drift ratio where the lateral strength decreases to 80% of its peak strength. Table 3 lists the capacity definition of the case column. The results in the table suggest that structural capacity decreases as corrosion time increases.

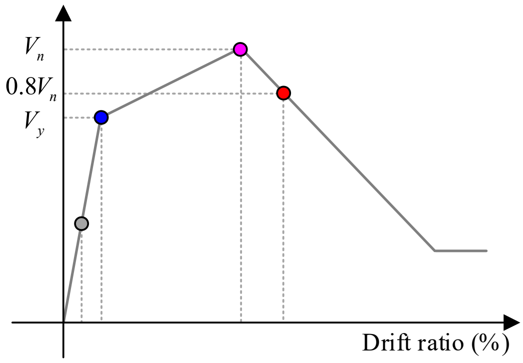

Fig. 17. Limit states definition for shear-critical columns.

Table 3
Damage limit states for corrosion columns (drift ratio: %).

Column	SD	MD	ED	CP
Pristine	0.11	0.22	0.50	1.20
25 years	0.11	0.21	0.50	1.17
50 years	0.10	0.20	0.48	1.16
75 years	0.09	0.18	0.44	1.14
100 years	0.09	0.16	0.41	1.12

7.4 Seismic fragility analysis

The analytical fragility functions express the conditional probability of attaining or exceeding a specified damage state under a certain set of ground motion intensity measures *IM* (e.g. PGA):

$$P[D > C \mid IM] = \Phi\left[\frac{\ln S_D - \ln S_C}{\sqrt{\beta_{IM}^2 + \beta_C^2}}\right] \tag{25}$$

where D and S_D are the seismic demand and median value, respectively; C and S_C are the seismic capacity and median value, respectively; β_{IM} and β_C are dispersion of the seismic demand and structural limit state, respectively. $\Phi(\cdot)$ is the cumulative normal distribution function. In this study, the S_C is obtained from the structural capacity analysis discussed above and the β_C is taken as 0.25 for the SD and MD damage states, 0.46 for ED and CP damage states according to [65].

The IDA method will be used in this paper to derive parameters of the fragility functions. From the IDA results, the seismic demand model that expresses the relationship between seismic demand of interested *EDP* and intensity measure *IM* can be obtained [66]:

$$EDP = a(IM)^b \text{ or } \ln(EDP) = \ln(a) + b\ln(IM) \tag{26}$$

where a and b are regression coefficients. The dispersion β_{IM} accounting for the uncertainty in the relationship is estimated as:

$$\beta_{IM} = \sqrt{\frac{\sum_{i=1}^{N}\left[\ln(EDP_i) - \ln(a(IM_i)^b)\right]^2}{N-2}} \tag{27}$$

where N is the total number of numerical simulations, EDP_i represents the demand of the ith simulation.

A suite of 22 far field ground motions are used in this study for the seismic fragility analysis. The 22 far field ground motions are selected from the FEMA-P695 far field ground motions set [67]. Detailed characteristics of the selected ground motion records are presented in Table A-2 in the Appendix. It should be noted that only the horizontal component of ground motions with larger PGA is used during the IDA.

7.5 Results and discussion

The effects of time-dependent corrosion and modeling methods on seismic drift demands of shear-critical RC columns are firstly assessed. Typical hysteretic responses of the bridge columns at different investigated times are shown in Fig. 18, where Fig. 18(a) illustrates hysteretic responses obtained using FSI-model, Fig. 18(b) shows the results obtained using flexure model. From Fig. 18(a), it can be seen that, due to the use of corrosion-induced reduced material properties, the drift demands of the bridge columns increase under the sample ground motion. The maximum drift ratio for the pristine column is 0.96%, while the drift demands will increase to 1.47% and 1.71% at 50 year and 100 year, respectively. Similar finding is obtained using the flexure-only model as illustrated in Fig. 18(b). The drift demand placed on the pristine column using the flexure model is 0.43%, and subsequently increases to 0.62% and 1.00% at 50 year and 100 year, respectively. The results also reveal that the modeling method for shear-critical columns has significant effect on drift demands. The FSI-model generates larger drift demands of columns at different investigated times, while using the flexure model which only accounts for flexure response tends to underestimate markedly the drift demands of shear-critical columns.

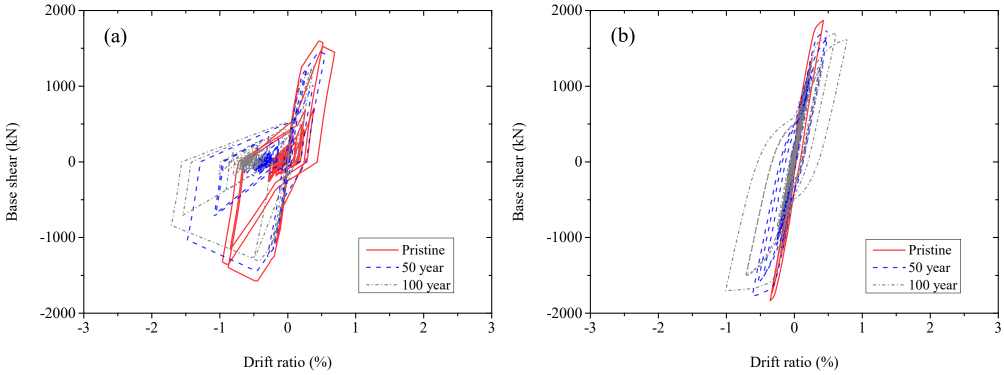

Fig. 18. Increase of drift demands for corroded columns under sample ground motion (NO. 18 in Table A-2 with PGA scaled to 0.5g): (a) FSI model; (b) flexure model.

Based on the above seismic fragility analysis framework, the time-dependent fragility curves for the shear-critical RC columns are obtained. Fig. 19 shows the analysis results of the fragility curves for the column case. The curves illustrate the probabilities of exceeding four damage states of the bridge column from 0 year to 100 year with a 25-year time interval. It can be seen that corrosion has slight effects with respect to light damage state, although the vulnerability for the damage state increase with increase in time. This is mainly because the column will experience damage at low ground motion intensities and as such the corrosion effect is not yet fully reflected. However, corrosion effects on seismic fragility becomes more pronounced at severer damage states, and marked increased probabilities of exceeding extensive damage state and collapse prevention damage state can be observed in Fig. 19(c) and (d). The median collapse capacity is approximately 0.63g for the pristine column, and the capacities will reduce to 0.54g and 0.50g at 50 years and 100 years, i.e. a reduction of 14.3% and 20.6%, respectively. The above results indicate that corrosion should be taken into consideration in structural seismic fragility assessment, especially for severer damage states.

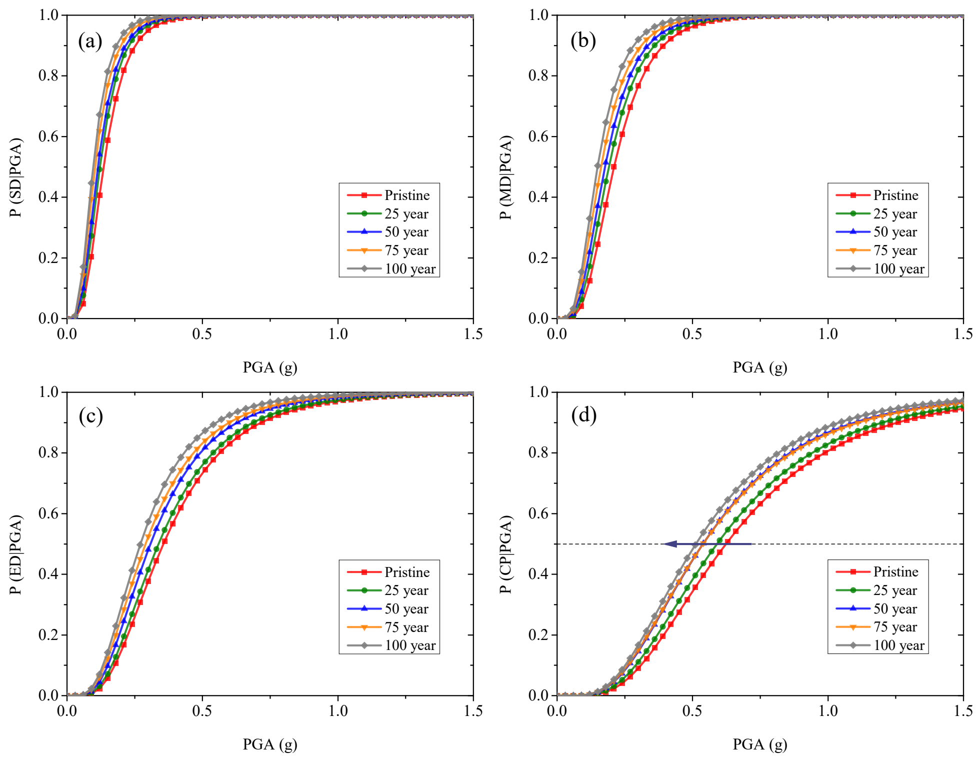

Fig. 19. Time-dependent fragility curves of shear-critical columns: (a) slight damage; (b) moderate damage; (c) extensive damage; (d) collapse prevention.

In order to compare the effectiveness of using the traditional method, which considers only flexure response and a time-invariant structural capacity index, and using the proposed evaluation method in this paper for the fragility analysis, the probability differences from using the two methods are also assessed. For the traditional method, the damage state definition are adopted from [51], which are taken as 0.5%, 1.0%, 2.0% and 2.5% for SD, MD, ED and CP damage states respectively. The analysis results are presented in Fig. 20, where the graphs on the left hand side show the comparison of seismic fragility curves using the two methods, and graphs on the right hand side show the probability differences over PGA.

It can be seen that the two methods generate significantly different fragility analysis results. Generally, the probability of exceeding a given damage state using the proposed method is much higher than that from the traditional method. The maximum probability difference could reach approximately 90% for the moderate damage state under around 0.3g for the studied column case. The traditional method underestimates the seismic fragility of the shear-critical columns as it ignores the deterioration in the shear performance, as well as in the structural capacities. The proposed method, which considers the differences in the longitudinal and transverse reinforcement corrosion over time and subsequently the time-dependent shear performance deterioration and the flexure-shear interaction behaviors both in structural capacities and seismic demands, reflects the increased seismic fragility for shear-critical columns.

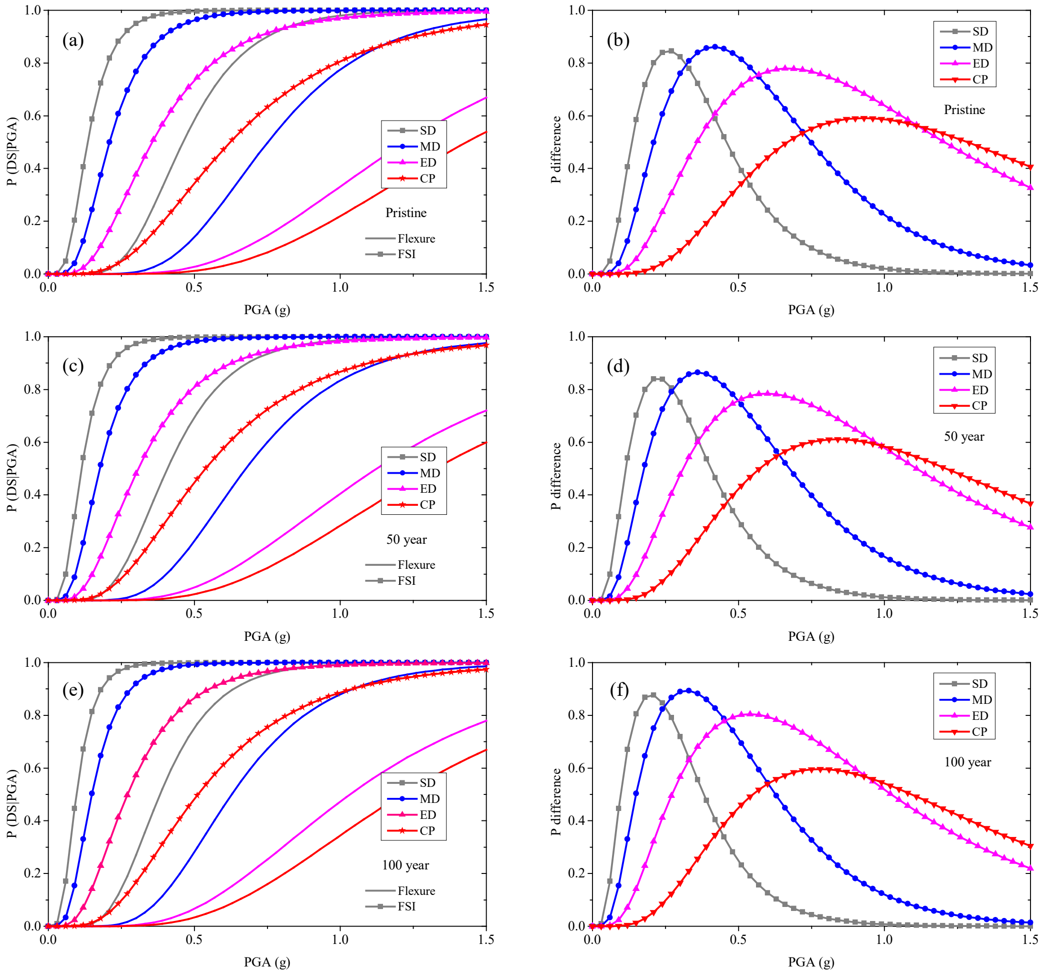

Fig. 20. Effects of evaluation methods on fragility analysis results of shear-critical column: (a), (b): pristine column; (c), (d): column at 50 years; (e), (f): column at 100 years (Left: seismic fragility curves; Right: probability difference).

8. Summary and conclusions

A framework for seismic fragility analysis for shear-critical reinforced concrete columns considering corrosion induced deterioration effects is presented in this paper. The framework comprises a corrosion modeling part which defines the corrosion initiation time and time-variant deteriorating material properties of the columns. Especially, the differences of corrosion levels between transverse and longitudinal steel reinforcements in reality are taken into account. A new model is proposed for corroded shear-critical columns to account for shear performance deterioration due to corrosion and the flexure-shear interaction behaviors of columns under seismic loadings. This is accomplished by introducing a new macro-spring element for shear response simulation in series with the nonlinear beam-column elements for flexure response and a zero-length section element for slip response at the base of the column. The modified Ibarra-Medina-Krawinkler deterioration model is adopted to simulate the shear response in order to capture shear strength and stiffness deterioration as well as pinching behavior of corroded shear-critical columns. The model is validated by comparing simulation results with experimental test results of shear-critical columns and the results indicate that the proposed model can reasonably simulate the hysteretic response of uncorroded shear-critical columns as well as corroded shear-critical columns. The proposed framework also adopts time-variant structural capacity for seismic fragility analysis where the time-dependent structural capacity is obtained with the proposed FSI-numerical model.

A representative bridge column is analysed to demonstrate the proposed framework and its effectiveness for time-dependent seismic fragility analysis for shear-critical columns. The results show that corrosion has significant effects on seismic fragility of the column, especially for severer damage states. The median collapse capacity is approximately 0.63g for the pristine column, and the capacities will reduce to 0.54g and 0.50g at 50 year and 100 year, with a reduction of 14.3% and 20.6%, respectively.

Comparison of the modeling methods indicates that, for corroded shear-critical columns, using the traditional flexure modeling method with time-invariant structural capacities tends to significantly underestimate the seismic fragility. The proposed method, which considers the differences in the longitudinal and transverse reinforcement corrosion over time, time-variant structural capacitie as well as time-dependent shear and flexure-shear interaction behaviors, reflects reasonably the increased seismic fragility for corroded shear-critical columns.

The proposed framework paves a way for more realistic seismic fragility analysis of shear-critical RC columns considering the effect of corrosion. Further work is required to extend the framework for the fragility analysis of other structure configurations, and calibration of the time-varying model parameters to cover different environmental and structural conditions.

ACKNOWLEDGMENTS

The authors acknowledge financial support from the National Natural Science Foundation of China (No. 51835004) and the National Key Research and Development Program of China (No. 2016YFC0701400, No. 2016YFC0701100). The opinions and conclusions presented in this paper are those of the authors and do not necessarily reflect the views of the sponsoring organizations.

Appendix A

Table A-1
Corrosion modeling parameters.

Parameter	Value	Unit
w/c	0.5	-
D_0	473	mm^2/year
k_e	0.924	-
k_t	0.832	-
k_c	1.0	-
t_0	28	day
n	0.362	-
A_{cs}	7.758	-
ε_{cr}	0	-
C_{cr}	0.9	mass % of binder

Note: C_{cs} is computed as: $C_{cs}=A_{cs}(w/c)+\varepsilon_{cr}$

Table A-2
Selected 22 far field ground motions.

NO.	Earthquake	M	Station	Epicentral distance (km)	PGA (g)	PGV (cm/s)
1	Northridge	6.7	Beverly Hills - Mulhol	13.3	0.52	63
2	Northridge	6.7	Canyon Country-WLC	26.5	0.48	45
3	Duzce, Turkey	7.1	Bolu	41.3	0.82	62
4	Hector Mine	7.1	Hector	26.5	0.34	42
5	Imperial Valley	6.5	Delta	33.7	0.35	33
6	Imperial Valley	6.5	El Centro Array #11	29.4	0.38	42
7	Kobe, Japan	6.9	Nishi-Akashi	8.7	0.51	37
8	Kobe, Japan	6.9	Shin-Osaka	46	0.24	38
9	Kocaeli, Turkey	7.5	Duzce	98.2	0.36	59

10	Kocaeli, Turkey	7.5	Arcelik	53.7	0.22	40
11	Landers	7.3	Yermo Fire Station	86	0.24	52
12	Landers	7.3	Coolwater	82.1	0.42	42
13	Loma Prieta	6.9	Capitola	9.8	0.53	35
14	Loma Prieta	6.9	Gilroy Array #3	31.4	0.56	45
15	Manjil, Iran	7.4	Abbar	40.4	0.51	54
16	Superstition Hills	6.5	El Centro Imp. Co.	35.8	0.36	46
17	Superstition Hills	6.5	Poe Road (temp)	11.2	0.45	36
18	Cape Mendocino	7.0	Rio Dell Overpass	22.7	0.55	44
19	Chi-Chi, Taiwan	7.6	CHY101	32	0.44	115
20	Chi-Chi, Taiwan	7.6	TCU045	77.5	0.51	39
21	San Fernando	6.6	LA - Hollywood Stor	39.5	0.21	19
22	Friuli, Italy	6.5	Tolmezzo	20.2	0.35	31

References

[1] Sezen H, Whittaker AS, Elwood KJ, Mosalam KM. Performance of reinforced concrete buildings during the august 17, 1999 Kocaeli, Turkey earthquake, and seismic design and construction practise in Turkey. Eng Struct 2003;25(1):103–14.

[2] Ramanathan KN. Next generation seismic fragility curves for California bridges incorporating the evolution in seismic design philosophy. Ph.D.thesis, Atlanta (GA): School of Civil and Environmental Engineering, Georgia Institute of Technology; 2012.

[3] Elnashai A, Sarno LD. Fundamentals of earthquake engineering. Wiley; 2008.

[4] Ma G, Li H, Hwang HJ. Seismic behavior of low-corroded reinforced concrete short columns in an over 20-year building structure. Soil Dyn Earthquake Eng 2018;106:90-100.

[5] Billah AHMM, Alam MS, Bhuiyan AR. Fragility analysis of retrofitted multicolumn bridge bent subjected to near fault and far field ground motion. J Bridge Eng 2013;18(10):992-1004.

[6] Liel AB. Assessing the collapse risk of California's existing reinforced concrete frame structures: Metrics for seismic safety decisions. Ph.D. thesis, Department of Civil and Environmental Engineering, Stanford University, CA;2008.

[7] Di Sarno, L. and F. Pugliese, Seismic performance of corroded reinforced concrete structures. Atti del XVIII Convegno ANIDIS L'ingegneria Sismica in Italia: Ascoli Piceno, 15-19 September 2019;101-108.

[8] Alipour A, Shafei B, Shinozuka M. Performance evaluation of deteriorating highway bridges located in high seismic areas. J Bridge Eng 2011;16(5):597-611.

[9] Choe D, Gardoni P, Rosowsky D, Haukaas T. Seismic fragility estimates for reinforced concrete bridges subject to corrosion. Struct Saf 2009;31(4):275-283.

[10] Choe D, Gardoni P, Rosowsky D, Haukaas T. Probabilistic capacity models and seismic fragility estimates for RC columns subject to corrosion. Reliab Eng Syst Saf 2008;93(3):383-393.

[11] Ghosh J, Padgett JE. Aging considerations in the development of timedependent seismic fragility curves. J Struct Eng 2010;136(12):1497-1511.

[12] Gidaris I, Padgett JE, Barbosa AR, Chen S, Cox D, Webb B, et al. Multiple-hazard fragility and restoration models of highway bridges for regional risk and resilience assessment in the United States: state-of-the-art review. J Struct Eng 2017;143(3):04016188.

[13] Cui F, Zhang H, Ghosn M, Xu Y. Seismic fragility analysis of deteriorating RC bridge substructures subject to marine chloride-induced corrosion. Eng Struct 2018;155:61-72.

[14] Yalciner H, Sensoy S, Eren O. Seismic performance assessment of a corroded 50-year-old reinforce concrete building. J Struct Eng 2015;27(6):683-696.

[15] Afsar Dizaj E, Madandoust R, Kashani MM. Probabilistic seismic vulnerability analysis of corroded reinforced concrete frames including spatial variability of pitting corrosion. Soil Dyn Earthq Eng 2018;114:97-112.

[16] Ghosh J, Sood P. Consideration of time-evolving capacity distributions and improved degradation models for seismic fragility assessment of aging highway bridges. Reliab Eng Syst Saf 2016;154:197-218.

[17] Celarec D, Vamvatsikos D, Dolšek M. Simplified estimation of seismic risk for reinforced concrete buildings with consideration of corrosion over time. Bull Earthq Eng 2011;9(4):1137-1155.

[18] Biondini F, Camnasio E, Titi A. Seismic resilience of concrete structures under corrosion. Earthquake Eng Struct Dyn 2015;44(14):2445-2466.
[19] Liu X, Jiang H, He L. Experimental investigation on seismic performance of corroded reinforced concrete moment-resisting frames. Eng Struct 2017;153:639-652.
[20] Ou YC, Fan HD, Nguyen ND. Long-term seismic performance of reinforced concrete bridges under steel reinforcement corrosion due to chloride attack. Earthquake Eng Struct Dyn 2013;42(14):2113-2127.
[21] Zhang Y, DesRoches R, Tien I. Impact of corrosion on risk assessment of shear-critical and short lap-spliced bridges. Eng Struct 2019;189:260-271.
[22] Feng D-C, Xu J. An efficient fiber beam-column element considering flexure–shear interaction and anchorage bond-slip effect for cyclic analysis of RC structures. Bull Earthq Eng 2018; 16(11): 5425-5452..
[23] Zimos DK, Mergos PE, Kappos AJ. Modelling of R/C members accounting for shear failure localisation: Hysteretic shear model. Earthquake Eng Struct Dyn 2018; 47(8): 1722-1741.
[24] Liu K-Y, Witarto W, Chang K-C. Composed analytical models for seismic assessment of reinforced concrete bridge columns. Earthquake Eng Struct Dyn 2015; 44(2): 265-281.
[25] LeBorgne MR, Ghannoum WM. Analytical element for simulating lateral-strength degradation in reinforced concrete columns and other frame members. J Struct Eng 2014; 140(7): 04014038.
[26] Baradaran Shoraka M, Elwood KJ. Mechanical model for non ductile reinforced concrete columns. J Earthquake Eng 2013; 17(7): 937-957.
[27] Kashani MM, Maddocks J, Dizaj EA. Residual capacity of corroded reinforced concrete rridge components: state-of-the-art review. J Bridge Eng 2019;24:03119001.
[28] Elwood KJ. Modelling failures in existing reinforced concrete columns. Can J Civ Eng 2004;31(5):846-59.
[29] O'Reilly GJ, Sullivan TJ. Modeling techniques for the seismic assessment of the existing Italian RC frame structures. J Earthquake Eng 2017; 23(8):1262-1296.
[30] Yuan W, Guo A, Li H. Seismic failure mode of coastal bridge piers considering the effects of corrosion-induced damage. Soil Dyn Earthq Eng 2017;93:135-146.
[31] Vu NS, Li B. Seismic performance of flexural reinforced concrete columns with corroded reinforcement. ACI Struct J 2018;111(5):1253-1266.
[32] Cheng H, Li H-N, Yang YB, Wang D-S. Seismic fragility analysis of deteriorating RC bridge columns with time-variant capacity index. Bull Earthq Eng 2019; 17(7): 4247-4267.
[33] Mazzoni S, McKenna F, Scott MH and Fenves GL. OpenSees command language manual. Pacific Earthquake Engineering Research (PEER) Center, 264; 2006.
[34] Ibarra LF, Medina RA, Krawinkler HA. Hysteretic models that incorporate strength and stiffness deterioration. Earthq Eng Struct Dyn 2005;34(12):1489-1511.
[35] Lignos, D.G. and H. Krawinkler. Deterioration Modeling of Steel Components in Support of Collapse Prediction of Steel Moment Frames under Earthquake Loading. J Struct Eng 2011;137(11): 1291-1302.
[36] Du Y, Clark L, Chan A. Effect of corrosion on ductility of reinforcing bars. Mag Concr Res 2005;57(7):407-419
[37] Du Y, Clark L, Chan A. Residual capacity of corroded reinforcing bars. Mag Concr Res 2005;57(3):135–47.
[38] Cairns J, Plizzari GA, Du Y, Law DW, Franzoni C. Mechanical properties of corrosion-damaged reinforcement. ACI Mater J 2005;102 (4):256-264.
[39] Hsu TT, Mo YL. Unified theory of concrete structures. United Kingdom: John Wiley and Sons Ltd; 2010.
[40] Molina FJ, Alonso C, Andrade C. Cover cracking as a function of rebar corrosion: Part 2-Numerical model. Mater Struct 1993;26(9):532-548.
[41] Scott BD, Park R, Priestley M. Stress-strain behavior of concrete confined by overlapping hoops at low and high strain rates. J Proc 1982;79(1):13–27
[42] Almusallam AA, Al-Gahtani AS, Aziz AR. Effect of reinforcement corrosion on bond strength. Constr Build Mater 1996;10(2):123-129.
[43] Lin H, Zhao Y, Ožbolt J, Hans-Wolf R. The bond behavior between concrete and corroded steel bar under repeated loading. Eng Struct 2017;140:390-405.
[44] Zhao J, Sritharan S. Modeling of strain penetration effects in fiber-based analysis of reinforced concrete structures. ACI Struct J 2007;104(2):133-141.
[45] Zhang X, Li B. Shear-strength capacity assessment of corroded reinforced concrete beam-column joints. J Perform Constr Facil 2018;32(5):04018067.
[46] Ghannoum WM. Experimental and analytical dynamic collapse study of a reinforced concrete frame with light transverse reinforcement. Department of Civil and Environmental Engineering, University of California, Berkeley; 2007.
[47] Vecchio FJ, Collins MP. The modified compression field theory for reinforced concrete elements subjected to shear. ACI J 1986;83(2):219-231.
[48] D'Ambrisi A, Filippou FC. Modeling of cyclic shear behavior in RC members. J Struct Eng 1999; 125(10): 1143-1150.

[49] Lee DH, Elnashai AS. Seismic analysis of RC bridge columns with flexure-shear interaction. J Struct Eng 2001; 127(5): 546-553.
[50] Xu S-Y, Zhang J. Hysteretic shear-flexure interaction model of reinforced concrete columns for seismic response assessment of bridges. Earthq Eng Struct Dyn 2011; 40(3): 315-337.
[51] Jeon J-S, Shafieezadeh A, Lee DH, Choi E, DesRoches R. Damage assessment of older highway bridges subjected to three-dimensional ground motions: characterization of shear-axial force interaction on seismic fragilities. Eng Struct 2015;87:47-57
[52] Bentz EC, Collins MP. Response-2000: Reinforced concrete sectional analysis using the modified compression field theory. 1998.
[53] Sezen H, Moehle JP. Shear strength model for lightly reinforced concrete columns. J Struct Eng 2004; 130(11): 1692-1703.
[54] Baradaran Shoraka M. Collapse assessment of concrete buildings: An application to non-ductile reinforced concrete moment frames. Ph.D. thesis, Department of Civil Engineering, The University of British Columbia, Canada;2013.
[55] Stevens NJ, Uzumeri SM, Collins MP. Reinforced concrete subjected to reversed cyclic shear-experiments and constitutive model. ACI Struct J 1991;88(2):135-146.
[56] Vecchio FJ. Towards cyclic load modeling of reinforced concrete. ACI Structural Journal. 1999;96:193-202.
[57] LeBorgne MR, Ghannoum WM. Calibrated analytical element for lateral-strength degradation of reinforced concrete columns. Eng Struct 2014;81:35-48.
[58] Rahnama M, Krawinkler H. Effects of soft soil and hysteresis model on seismic demands. Rep. No. 108, John A. Blume Earthquake Engineering Center, Stanford Univ., Stanford, CA.
[59] Wang Z, Wang J, Xiu H, Liu T. Hysteretic model for reinforced concrete rectangular bridge columns with flexure-shear failure mode. China Journal of Highway and Transport. 2017;30(12):129-138. (in Chinses)
[60] Sezen H, Moehle JP. Seismic tests of concrete columns with light transverse reinforcement. ACI Structural Journal. 2006; 103(6): 842-849.
[61] Lee HS, Kage T, Noguchi T, Tomosawa F. An experimental study on the retrofitting effects of reinforced concrete columns damaged by rebar corrosion strengthened with carbon fiber sheets. Cem Concr Res 2003;33(4):563-70.
[62] Kashani Mohammad M, Lowes Laura N, Crewe Adam J, Alexander Nicholas A. Computational modelling strategies for nonlinear response prediction of corroded circular RC bridge piers. Adv Mater Sci Eng 2016;2016:1-15.
[63] Afsar Dizaj E, Madandoust R, Kashani MM. Exploring the impact of chloride-induced corrosion on seismic damage limit states and residual capacity of reinforced concrete structures. Struct Infrastruct Eng 2018;14(6):714-729.
[64] Vamvatsikos D, Cornell CA. Incremental dynamic analysis. Earthq Eng Struct Dyn 2002; 31(3): 491-514.
[65] Nielson BG, DesRoches R. Seismic fragility methodology for highway bridges using a component level approach. Earthq Eng Struct Dyn 2007; 36(6): 823-839.
[66] Cornell CA, Jalayer F, Hamburger RO, Foutch DA. Probabilistic basis for 2000 SAC federal emergency management agency steel moment frame guidelines. J Struct Eng 2002; 128(4): 526-533.
[67] FEMA P-695. Quantification of building seismic performance factors. In: prepared by Applied technology council for the federal emergency managementagency, Washington DC; 2009.